Supplementary Materials

Imported Wild-Type Poliovirus in Germany: A Modelling Study of Outbreak Potential

Table of Contents

1 Seroprotection

1.1 Routine Polio-Neutralization Data from Diagnostic Laboratories

To determine neutralizing antibody levels, a microneutralization assay was conducted following WHO protocols with minor adaptations. Either Vero (ATCC CCL-81) or HEp2 (ATCC CCL-23) cell lines were used. The assay used 100 tissue culture infective doses (100 $TCID_{50}$) of Sabin poliovirus type 1 strain. Prior to testing, serum samples underwent heat inactivation at 56°C for 30 minutes. Dilution protocols differed by diagnostic laboratory:

- Frankfurt: twofold serial dilutions from 1:10 to 1:1280. Samples were tested in triplicates.
- Stuttgart: twofold serial dilutions from 1:8 to 1:1024. Samples were tested in duplicates.

In both laboratories, a reference serum of known neutralising activity was used as a positive control. The data with measurement from 2005 to 2020 was used in another research project and publication [1]. The data set used in this project covers measurements from the years 2016 to 2022.

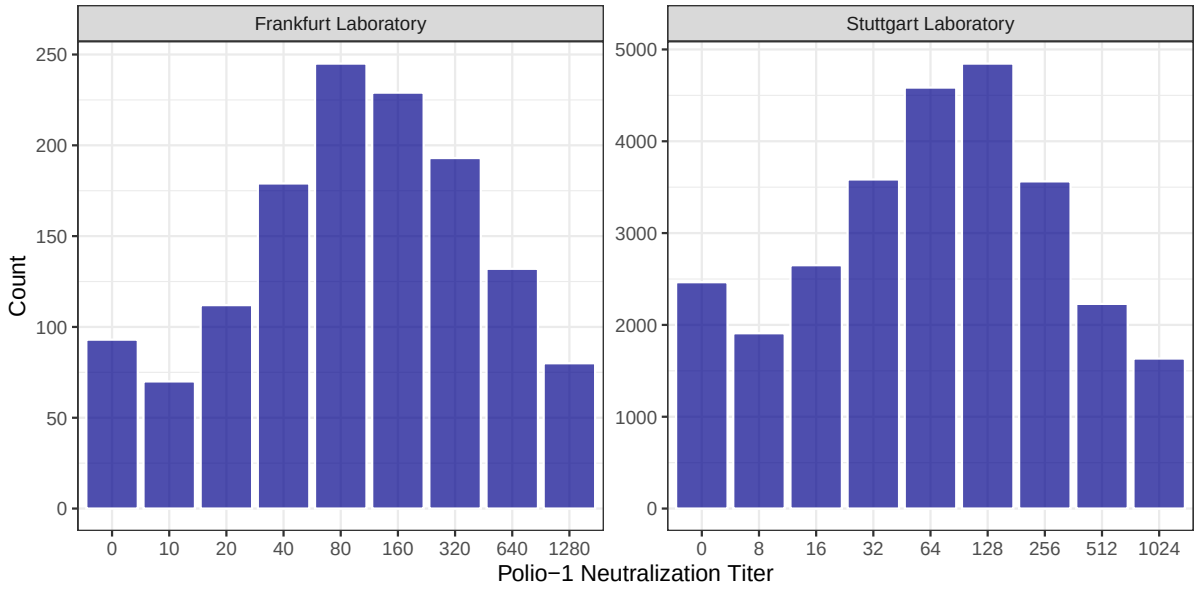

Figure S1: Distribution of polio neutralization titers by diagnostic laboratory.

Table S1: Distribution of measurements and protected fractions across grouped birth years. A titer of >1:10 (Frankfurt) or 1:8 (Stuttgart) was defined as sufficiently protected. The confidence intervals were calculated with the Wilson score method.

	Frankfurt Laboratory		**Stuttgart Laboratory**	
Birth Cohort	N	Protected Fraction (95% CI)	N	Protected Fraction (95% CI)
<1940	11	81.8% (52.3-94.9%)	399	82.7% (78.7-86.1%)
1940-1949	16	93.8% (71.7-98.9%)	1551	86.0% (84.2-87.6%)
1950-1959	68	98.5% (92.1-99.7%)	3708	88.9% (87.8-89.8%)
1960-1969	171	95.3% (91.0-97.6%)	5694	88.0% (87.1-88.8%)
1970-1979	277	96.0% (93.0-97.8%)	4731	87.5% (86.6-88.4%)
1980-1989	268	94.4% (91.0-96.6%)	4441	86.2% (85.1-87.2%)
1990-1999	377	93.6% (90.7-95.7%)	3790	80.4% (79.2-81.7%)
2000-2007	145	78.6% (71.3-84.5%)	3151	66.8% (65.1-68.4%)

1.2 Methods: Estimated Sero-Protection by Birth Cohort

The aim of this model was to estimate a continuous seroprotection curve across birth years in Germany. The model estimates the probability of being seroprotected against polio type 1 as a function of birth year. We include birth years from 1925 to 2022 in the model, and birth years were transformed to age (in years) relative to the ytear 2022. Three sources of information were combined into one Bayesian generalized additive model. First, vaccination coverage data from the Robert Koch Institute (RKI), as described in 1.1., was used to estimate seroprotection levels of children. Seroconversion rates and their 95%CIs were taken from two meta-analyses [2, 3]. Second, individual-level data from neutralization assays from two large German laboratories was used to estimate the seroprotection curve for birth years earlier than 2008. Third, two previously published studies were used to set weakly informative priors on the fraction of sero-protected adults [4, 5]. A historic, representative sero-survey found 96.2% of adults to be protected [4], and another survey found 93.3% to recall one or more polio vaccinations, with 75.1% having at least one documented dose [5]. We used these estimates for a uniform prior in older birth years.

To model potential changes in sero-protection but prevent implausible sudden shifts, we used a Bayesian Generalized Additive Model (GAM).

- **Spline predictor:** The GAM uses a cubic B-Spline with three basis functions (generated via R's splines package) to model sero-protection trends smoothly across birth years. The model estimated an overall intercept and specific beta (β) coefficients for the basis functions. These were combined to form the linear predictor (η) on the log-odds scale.
- **Likelihood and Link Function:** The spline's log-odds predictor (η) is mapped to a Bernoulli likelihood with an inverse-logit link function.
- **Routine Vaccination Coverage:** For the 2008–2022 birth year cohorts, the model calculates expected sero-protection by multiplying the vaccination coverage with literature-derived sero-conversion rates [2, 3]. The conversion rate is treated as a parameter informed by means and standard errors. For these birth years, the spline is closely anchored to the estimated sero-protection ($\sigma = 0.01$).
- **Neutralization-Test:** To estimate sero-protection for the birth years 1925 to 2007 we used routine, individual-level polio neutralization assay data from two diagnostic laboratories. The observations were classified into a binary (whether a person is above the seroprotection threshold or not) and modelled using a Bernoulli likelihood, which maps each person's status to the spline matrix based on their birth year. We used a uniform, weakly informative prior on the sero-protection rate across age groups that was informed by two surveys [4, 5].
- **Temporal Smoothing:** Since abrupt shifts in the seroprotection curve across birth years are unlikely, we used a first-order random walk prior on the linear predictor across consecutive birth years. By setting the change in log-odds from one birth year to the next to a normal distribution with a mean of zero and $\sigma = 0.05$, we assume that changes in coverage happen smoothly across birth cohorts.

Table S2: Assumed seroconversion rates for IPV vaccination schedules. For children born after 2008 we have data on the number of received vaccinations and used the conversion rates below.

Vaccination Schedule	**Estimate (95%CI)**	**References**
1 dose of IPV	0.33 (0.1-0.5)	[3]
2 doses of IPV	0.95 (0.9-0.97)	[2]
3 doses of IPV	0.96 (0.93,0.98)	[2]

Table S3: Priors in the sero-protection model.

Prior	**Distribution**	**Comments & References**
α	$\mathcal{N}(2,1)$	Intercept and baseline log-odds of seroprotection. Centered at 2 ($\text{logit}^{-1}(2) \approx 88\%$) based on prior domain knowledge of high baseline protection.
β_{raw}	$\mathcal{N}(0,1)$	Unscaled spline weights. Non-centered reparameterization ($\beta = \sigma_\beta \cdot \beta_{\text{raw}}$); equivalent to Normal$(0, \sigma_\beta)$ but reduces funnel geometry and sampling divergences [6].
σ_β	Exp(1)	Standard deviation of spline coefficients. For smoothness and penalization of unnecessary function complexity [7].
ρ	$\mathcal{N}(0, 0.05)$	Year-to-year change in the linear predictor ($\eta_i - \eta_{i-1} \sim \rho$). The first order random walk prior ρ is for a smooth transition across consecutive birth cohorts [8].

1.3 Results: Estimated Sero-Protection by Birth Cohort

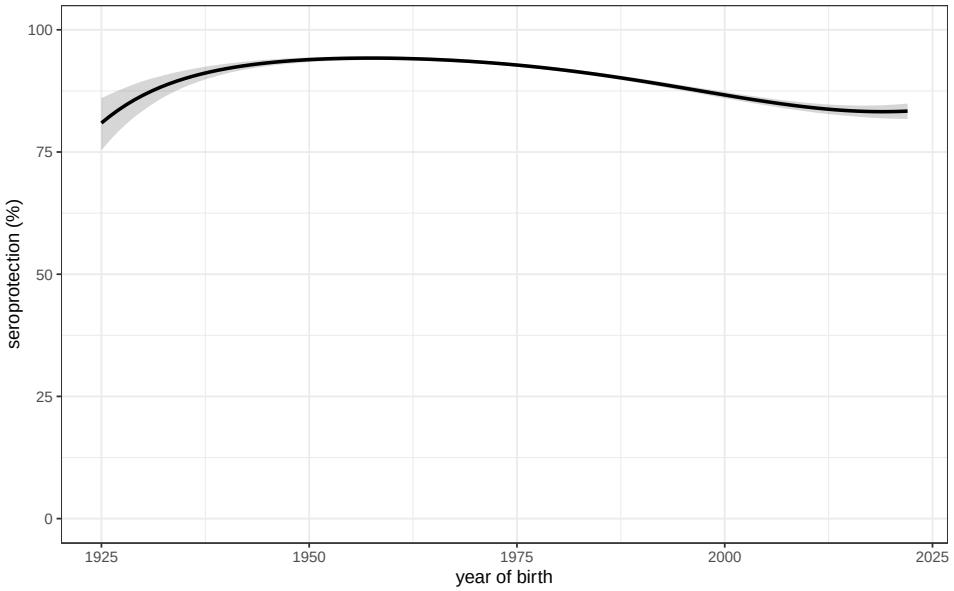

Figure S2: In black the spline function of birth year cohort and the estimated sero-protected fraction of the population. In grey the 95% credible interval (CrI). This continuous estimate was discretized into age groups to inform the age-stratified transmission model.

2 Transmission Model

2.1 Equations

Table S4: Look-up table of the model's state variables and parameters.

Symbol	Definition
Subscripts and Indices	
g, h	Indices for age groups
k	Index for Erlang infectious stage ($k \in \{1, 2, 3\}$)
m	Prior immunity status: Susceptible (s), IPV-vaccinated (i), OPV-vaccinated (o)
c	Clinical manifestation: Asymptomatic (a), Symptomatic/Disease (d)
State Variables and Vectors	
N	Total population
S	Susceptible individuals
V_m	Vaccinated individuals by immunity status $m \in \{i, o\}$
E_m	Exposed (latent) individuals by prior immunity status $m \in \{s, i, o\}$
$I_{c,m}^{(k)}$	Infected individuals of symptom and susceptibility status c and m at Erlang stage k (Note: Only $c = a$ exists for $m \in \{i, o\}$; both $c \in \{a, d\}$ exist for $m = s$)
$\mathbf{I}$	Vector of all infectious states across all age groups
R	Recovered individuals
Parameters	
b_g	Crude birth rate into age group g ($b_g = 0$ for $g > 1$)
ν_g	Per-capita vaccination rate of susceptible individuals ($\nu_g = 0$ for $g > 1$)
$\lambda_m(\mathbf{I})$	Force of infection by prior immunity status $m \in \{s, i, o\}$
σ	Transition rate from exposed to infectious classes (inverse of latent period)
p_s	Probability of developing an asymptomatic infection for unvaccinated individuals
$\gamma_{c,m,k}$	Progression rate out of Erlang stage k by symptom and susceptibility status c and m
μ	Background per-capita mortality rate
μ_d	Total mortality rate for symptomatic individuals (μ + disease-induced mortality)
$\beta(t)$	Seasonal transmission rate
$C_{g,h}$	Contact matrix elements representing rate of contact between age groups g and h
θ_m	Relative susceptibility modifier based on prior immunity status m (with $\theta_s = 1.0$)
$\rho_{c,m,k}$	Relative infectiousness (shedding) by clinical, immunity, and Erlang stage status

In the following system of ordinary differential equations, we omit the ageing terms for clarity. The system of equations for uninfected susceptible, IPV/OPV vaccinated, and exposed individuals are such that

$$\frac{dS_g}{dt} = b_g - \nu_g S_g - \lambda_{s,g}(t, \mathbf{I}) S_g - \mu S_g \tag{1}$$

$$\frac{dV_{i,g}}{dt} = \nu_g S_g - \lambda_{i,g}(t, \mathbf{I}) V_{i,g} - \mu V_{i,g} \tag{2}$$

$$\frac{dV_{o,g}}{dt} = -\lambda_{o,g}(t, \mathbf{I}) V_{o,g} - \mu V_{o,g} \tag{3}$$

$$\frac{dE_{s,g}}{dt} = \lambda_{s,g}(t, \mathbf{I}) S_g - \sigma E_{s,g} - \mu E_{s,g} \tag{4}$$

$$\frac{dE_{i,g}}{dt} = \lambda_{i,g}(t, \mathbf{I}) V_{i,g} - \sigma E_{i,g} - \mu E_{i,g} \tag{5}$$

$$\frac{dE_{o,g}}{dt} = \lambda_{o,g}(t, \mathbf{I}) V_{o,g} - \sigma E_{o,g} - \mu E_{o,g}, \tag{6}$$

where $\mathbf{I}$ denotes the vector of all infectious states across age groups.

The infectious stages follow an Erlang-distribution to model time-varying shedding. For infected individuals originating from the susceptible class (S), the transitions into asymptomatic (a) or symptomatic (d) pathways are expressed as

$$\frac{dI^{(1)}_{a,s,g}}{dt} = p_s \sigma E_{s,g} - (\gamma_{a,s,1} + \mu) I^{(1)}_{a,s,g} \tag{7}$$

$$\frac{dI^{(k)}_{a,s,g}}{dt} = \gamma_{a,s,k-1} I^{(k-1)}_{a,s,g} - (\gamma_{a,s,k} + \mu) I^{(k)}_{a,s,g} \quad \text{for } k \in \{2, 3\} \tag{8}$$

$$\frac{dI^{(1)}_{d,s,g}}{dt} = (1 - p_s) \sigma E_{s,g} - (\gamma_{d,s,1} + \mu_d) I^{(1)}_{d,s,g} \tag{9}$$

$$\frac{dI^{(k)}_{d,s,g}}{dt} = \gamma_{d,s,k-1} I^{(k-1)}_{d,s,g} - (\gamma_{d,s,k} + \mu_d) I^{(k)}_{d,s,g} \quad \text{for } k \in \{2, 3\} \tag{10}$$

For infected individuals originating from the vaccinated classes (V_i and V_o), transition through asymptomatic infection stages follows

$$\frac{dI^{(1)}_{a,i,g}}{dt} = \sigma E_{i,g} - (\gamma_{a,i,1} + \mu) I^{(1)}_{a,i,g} \tag{11}$$

$$\frac{dI^{(k)}_{a,i,g}}{dt} = \gamma_{a,i,k-1} I^{(k-1)}_{a,i,g} - (\gamma_{a,i,k} + \mu) I^{(k)}_{a,i,g} \quad \text{for } k \in \{2,3\} \tag{12}$$

$$\frac{dI^{(1)}_{a,o,g}}{dt} = \sigma E_{o,g} - (\gamma_{a,o,1} + \mu) I^{(1)}_{a,o,g} \tag{13}$$

$$\frac{dI^{(k)}_{a,o,g}}{dt} = \gamma_{a,o,k-1} I^{(k-1)}_{a,o,g} - (\gamma_{a,o,k} + \mu) I^{(k)}_{a,o,g} \quad \text{for } k \in \{2,3\} \tag{14}$$

The dynamics of the recovered compartment were derived to follow

$$\frac{dR_g}{dt} = \gamma_{a,s,3} I^{(3)}_{a,s,g} + \gamma_{d,s,3} I^{(3)}_{d,s,g} + \gamma_{a,i,3} I^{(3)}_{a,i,g} + \gamma_{a,o,3} I^{(3)}_{a,o,g} - \mu R_g. \tag{15}$$

The force of infection on individuals in age group g with immunity status $m \in \{s, i, o\}$ was derived as

$$\lambda_{m,g}(t, \mathbf{I}) = \theta_m \beta(t) \sum_h C_{g,h} \frac{\sum_{k=1}^{3} \left(\rho_{a,s,k} I^{(k)}_{a,s,h} + \rho_{d,s,k} I^{(k)}_{d,s,h} + \rho_{a,i,k} I^{(k)}_{a,i,h} + \rho_{a,o,k} I^{(k)}_{a,o,h} \right)}{N_h} \tag{16}$$

where $C_{g,h}$ is the age-structured contact matrix and θ_m is the relative susceptibility of group m (where for susceptibles $\theta_s = 1.0$). The relative shedding (infectiousness) of individuals based on their clinical state, prior immunity, and infectious stage was simplified into $\rho_{c,m,k}$. The seasonal transmission rate $\beta(t)$ is such that

$$\beta(t) = \beta \left(1 + f \times \cos \left(\frac{2\pi(t - \phi)}{365} \right) \right), \tag{17}$$

where f is the seasonal forcing amplitude and ϕ is the phase shift.

2.2 Parameters

Table S5: Parameters for the polio model. We used the best estimates to calibrate our model for the primary analyses. Their plausible ranges were used in Latin Hypercube Sampling.

Parameter	Best Estimate	Range	References
Basic reproduction number R_0	3.0	1.5-5	[9–11, 11–14]
Latent period (days)	3	2-6	[15, 16]
Probability of AFP	1/200	–	[17]
Total mortality rate of AFP	10%	–	[17]
Total shedding duration (days)			[13, 18, 19]
Susceptibles	29	28-35	
IPV vaccinated	18	18-29	
Relative duration of infection stages			[13, 18]
Stage 1	$4/29$	–	
Stage 2	$3/29$	–	
Stage 3	$22/29$	–	
Relative shedding intensity in infection stages (relative to the second stage)			[13, 18]
Stage 1	$10^{1.3}/10^{2.5}$	$10^{1.3}/10^{2.5}$-1	
Stage 2	1	–	
Stage 3	$10^{1.3}/10^{2.5}$	$10^{1.3}/10^{2.5}$-1	
IPV effectiveness against infection	30%	20-40%	[18, 20, 21]
Infectiousness of IPV vaccinated persons (relative to susceptibles)	0.25	0.1-0.5	[14, 18]
Seasonal forcing amplitude	0.35	0-0.7	[22, 23]
Peak transmission (calendar day)	270	200-300	[22, 24]
Rate of completing polio immunization within the first 5 years of life	88%	–	[25]

Table S6: There is uncertainty around polio transmission parameters in high-hygiene, northern countries. We provide an extended justification for some parameter choices.

Parameter	Justification
R_0	We chose R_0 based on data from high-hygiene settings [14]. The same choice was made in prior modelling studies for polio-free settings [9, 10]. Studies of the 2013 WPV1 outbreak in Israel estimated $R_0 \approx 1.5$ [11–13]. However, their models may have underestimated R_0 by not accounting for prior IPV immunity in the population. We wanted to err on the side of caution regarding outbreak potential and used the established estimate [9, 10, 14].
Shedding duration/intensity	There is evidence of shorter durations of fecal shedding in IPV vaccinated persons [14, 21]. For low-shedding phases of WPV1 infection, we used the relative shedding intensity estimated by Brouwer et al. [13].
IPV relative infectiousness	There is evidence of much smaller amounts of fecal shedding in IPV vaccinated persons [14]. But there is lack of empirical evidence how this reduction in shedding translates to reduced infectiousness of IPV vaccinated persons. We therefore draw our parameter from an expert elicitation study [18]. Parameters from this expert elicitation have been used by prior studies for the calibration of their polio models [13, 20, 22, 26].
IPV protection against infection	Similarly, the effectiveness of IPV vaccination against infection remains unclear. While it probably offers very little protection against fecal-oral transmission, it probably offers protection against oro-pharyngeal transmission, which is assumed to be an important transmission pathway in high-hygiene countries [14, 18, 21, 27, 28]. We therefore use the expert elicitation study's estimate of the protection of IPV against all transmission [18], which have been used in existing polio models [20, 22, 29]. We further validate the IPV related parameters in our sensitivity analysis with the outbreak data from Israel.
Seasonality of transmission	Like most enteroviruses, polio transmission follows seasonal fluctuation, with a probable peak in late summer or autumn in Germany [23, 24]. We assumed the same seasonal force and timing as a polio model for the Netherlands [20]. A modeling study from Israel [11] derived their seasonality parameters from US data [23]. We did not follow their approach, since Germany is much warmer compared to US states of similar latitude [30].

2.3 Vaccine Hesitant Sub-Population

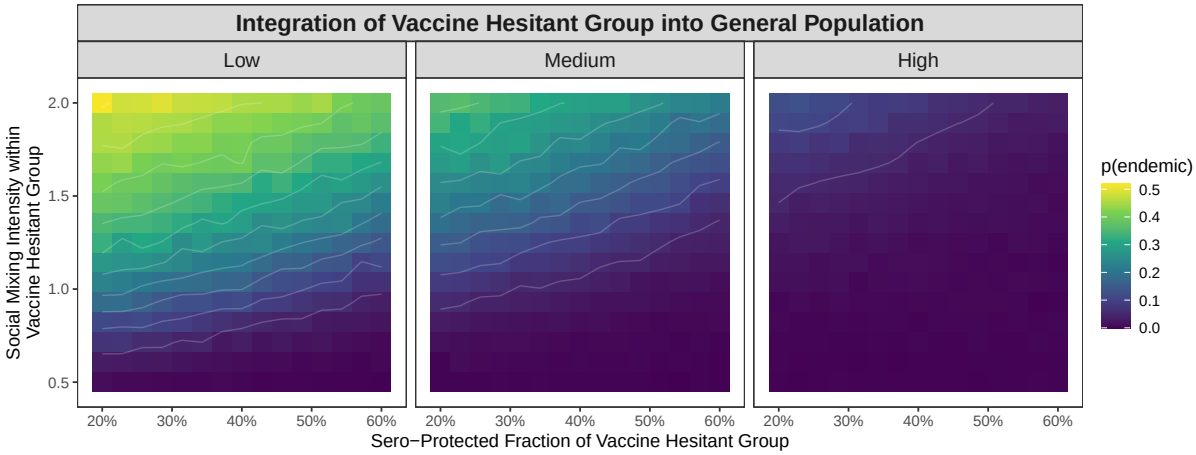

Figure S3: Probability of endemic WPV1 transmission following its introduction into a vaccine-hesitant subgroup. Across three levels of integration of the subgroup into the general population, we estimate how within-group mixing and the fraction of susceptible individuals affect the probability of endemicity. This is the un-smoothed grid search. In the main text, we used a Generalized Additive Model to generate a smooth response surface from this data. This was done to smooth out stochastic noise and reduce the computational costs of higher-resolution grid searching.

2.4 Sensitivity Analyses

2.4.1 Global Sensitivity Analysis

We conducted a global sensitivity analysis using the Sobol-Jansen method to evaluate how parameter uncertainty affects the primary model outcome, the probability of one or AFP cases following importation. Input parameter spaces were defined using independent uniform distributions over plausible parameter ranges (see table S5).

For the $d = 9$ evaluated parameters, we drew two independent sample sets of size $n_p = 1,024$ from the plausible parameter space. From this, we constructed a Sobol matrix with a total of $n_p \times (d + 2) = 11,264$ parameter permutations. For each permutation, the model was run for 2,500 stochastic repetitions. We calculated first-order (S_i) and total-order (S_{Ti}) Sobol indices to quantify, respectively, the direct main effects of individual parameters and their overall contributions including higher-order parameter interactions to the probability of endemic transmission. The 95% confidence intervals were estimated using non-parametric bootstrapping with $10,000$ resamples.

Table S7: Global sensitivity analysis with first and total order sobol indices for the outcome of AFP cases following importation. The 95% bootstrap confidence intervals are shown in brackets. See a visualization on the next page.

Parameter	**First Order Sobol (95%CI)**	**Total Order Sobol (95%CI)**
R0 Estimate	0.432 (0.357-0.518)	0.734 (0.646-0.812)
Relative shedding (IPV)	0.259 (0.167-0.364)	0.525 (0.455-0.589)
Time-varying shedding	-0.008 (-0.107-0.104)	0.059 (0.045-0.072)
IPV protection against infection	0.028 (-0.060-0.128)	0.041 (0.032-0.048)
Shedding duration (IPV vaccinated)	-0.001 (-0.088-0.097)	0.008 (0.006-0.010)
Sigma (latent period)	-0.003 (-0.090-0.095)	0.004 (0.003-0.005)
Shedding duration (Susceptibles)	-0.006 (-0.094-0.093)	0.002 (0.001-0.002)
Seasonal phase shift	-0.004 (-0.092-0.093)	0.001 (0.001-0.001)
Seasonal forcing	-0.002 (-0.089-0.096)	0.001 (0.001-0.001)

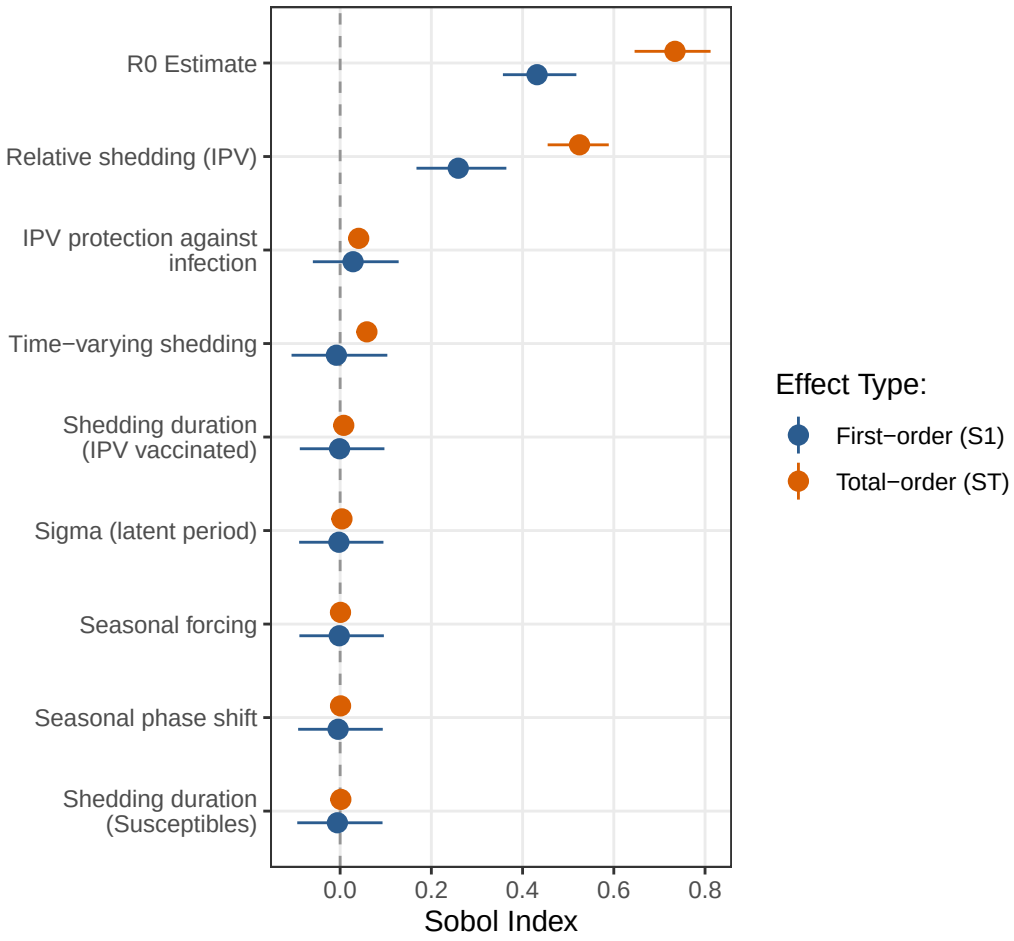

Figure S4: Global sensitivity analysis and first and total order sobol indices for the primary outcome of the probability of AFP cases. The point estimates are shown as dots, and the 95% bootstrap confidence intervals are shown as error bars. The highest variation comes from the choice of R0 and the relative shedding intensity of IPV vaccinated persons. A grid search was done to estimate their impact on the outcome. See next page.

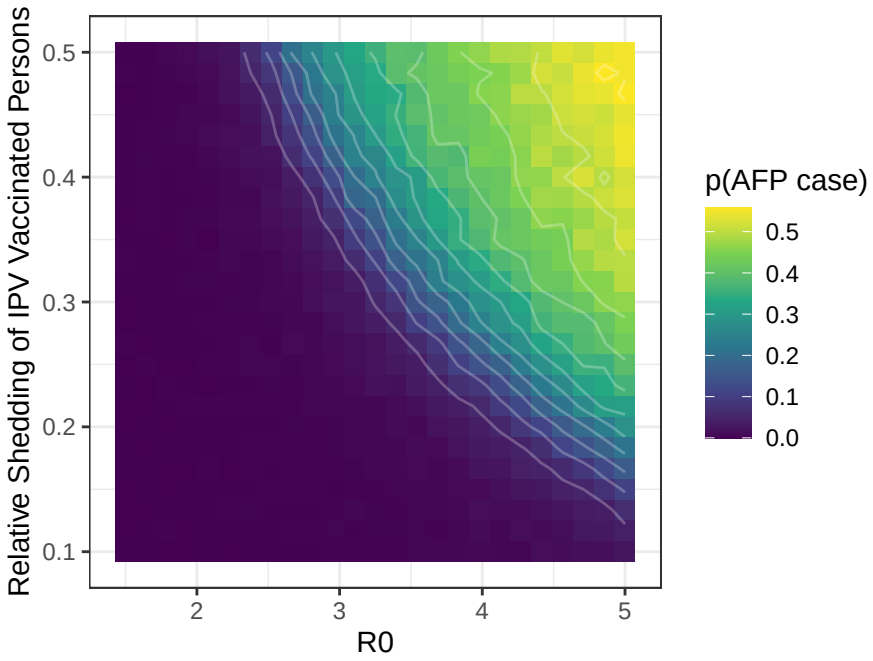

Figure S5: Probability of at least one AFP case, depending on assumed R_0 and viral shedding intensity by IPV vaccinated persons. Based on the results of the Sobol variance analysis, we conducted a grid search of the highest-impact parameters. The model was run on a 25×25 grid of relative shedding intensities of IPV vaccinated persons (compared to susceptibles) and the R_0 estimate. For each parameter combination, the model was run for 2,500 stochastic repetitions.

2.4.2 Alternative Importation Scenarios

We modelled different, plausible importation scenarios.

- **Reference Scenario:** Reference Scenario. Arrival of 1 unvaccinated infected child aged 0-4 years old in the late stage of WPV1 infection.
- **Scenario 1** Arrival of 1 unvaccinated infected child aged 0-4 years old in the *early stage* of WPV1 infection.
- **Scenario 2:** Arrival of 1 unvaccinated infected child aged 0-4 years and 1 adult aged 20-29 years old. Both unvaccinated and in the late, long-shedding stage if WPV1 infection.
- **Scenario 3:** Arrival of 1 IPV-vaccinated adult aged 20-29 years old in a late stage of WPV1 infection.

Table S8: WPV1 Importation scenarios and the predicted model outcome of probability of endemic transmission, the probability of one or more cases of AFP, and the expected number of days until all transmission ceases.

	Endemicity (95%PI)	**AFP Case (95%PI)**	**Extinction Time (IQR)**
Reference	0.80% (0.49-1.23%)	0.68% (0.40-1.09%)	24.0 days (8-73)
Scenario 1	3.88% (3.16-4.71%)	3.64% (2.94-4.45%)	96.0 days (43-173)
Scenario 2	1.60% (1.15-2.17%)	1.36% (0.94-1.90%)	59.0 days (25-131)
Scenario 3	0.24% (0.09-0.52%)	0.28% (0.11-0.58%)	11.0 days (5-25)

Table S9: We used our reference scenario for WPV1 but varied the age group of the index case. The predicted model outcomes of probability of endemic transmission, the probability of one or more cases of AFP, and the expected number of days until all transmission ceases are shown. The prediction intervals of the scenarios overlap, suggesting no significant difference.

Seed Age	**Endemicity (95%PI)**	**AFP Case (95%PI)**	**Extinction Time (IQR)**
[0, 5) years	0.80% (0.49-1.23%)	0.68% (0.40-1.09%)	24.0 days (8-73)
[5, 10) years	0.72% (0.43-1.14%)	1.20% (0.81-1.71%)	24.0 days (8-64)
[10, 15) years	1.16% (0.78-1.66%)	1.52% (1.08-2.08%)	28.0 days (9-92)
[15, 20) years	1.88% (1.38-2.49%)	1.76% (1.28-2.36%)	34.0 days (9-119)
[20, 30) years	0.88% (0.55-1.33%)	0.64% (0.37-1.04%)	25.0 days (8-73)
[30, 40) years	0.80% (0.49-1.23%)	1.04% (0.68-1.52%)	28.0 days (8-76)
[40, 50) years	0.80% (0.49-1.23%)	1.00% (0.65-1.47%)	30.0 days (9-83)
[50, 60) years	0.32% (0.14-0.63%)	0.60% (0.34-0.99%)	22.0 days (7-57)
[60, Inf) years	0.28% (0.11-0.58%)	0.44% (0.22-0.79%)	19.0 days (7-44)

2.4.3 Seasonality and Timing of Importation

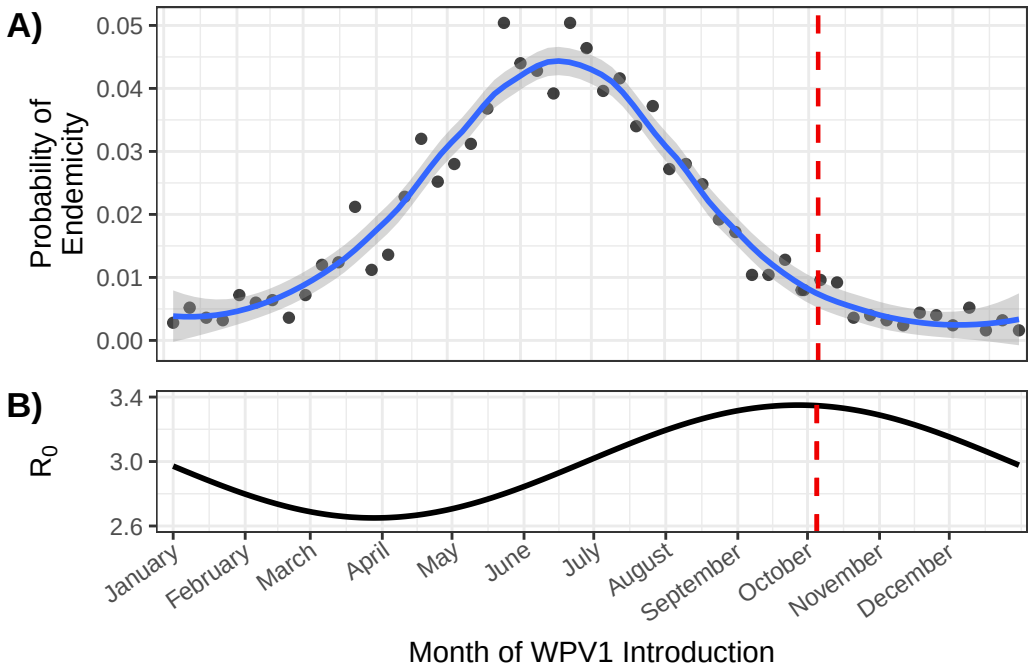

Figure S6: Impact of WPV1 introduction timing and seasonal forcing on the probability of endemic transmission (defined as transmission for 365 days or longer). In both panels, the red dashed line marks the date of introduction that was used in the main importation scenario of this study (October 05). **A)** Probability of endemic transmission following importation. The estimate for each importation date was plotted with black dots. We simulated an introduction for every calendar week of the year, and ran 2,500 stochastic repetitions for each importation time point using the reference scenario. Locally estimated scatterplot smoothing was used to draw the blue trend line. **B)** Amplitude of the seasonally forced R_0. See equation 17 for the derivation, as well as tables S5 and S6 for the parametrization.

2.4.4 Historic OPV Vaccination

We modeled the potential impact of OPV vaccination in three plausible scenarios. The results of them are compared to the reference importation scenario, where we assume OPV vaccination pre-1998 to make no difference compared to IPV vaccination.

- **Reference Scenario:** Reference Scenario. Arrival of 1 unvaccinated infected child aged 0-4 years old in the late stage of WPV1 infection.
- **OPV Scenario 1:** Historic OPV vaccination reduces susceptibility to WPV1 infection (50% relative to unvaccinated persons [18]).
- **OPV Scenario 2:** Historic OPV vaccination reduces WPV1 shedding (90% less shedding relative to unvaccinated persons [18]).
- **OPV Scenario 3:** Historic OPV vaccination reduces susceptibility to infection *and* shedding.

	Endemicity (95%PI)	**AFP Case (95%PI)**	**Extinction Time (IQR)**
Reference	0.80% (0.49-1.23%)	0.68% (0.40-1.09%)	24.0 days (8-73)
OPV Scenario 1	0.16% (0.04-0.41%)	0.72% (0.43-1.14%)	24.0 days (8-61)
OPV Scenario 2	0.08% (0.01-0.29%)	0.56% (0.31-0.94%)	24.0 days (8-60)
OPV Scenario 3	0.00% (0.00-0.15%)	0.32% (0.14-0.63%)	23.5 days (8-54)

2.4.5 Only Children < 15 Years

In this sensitivity analysis, we only used national vaccination coverage data, which is available for children born between 2008 and 2022, and we modeled transmission dynamics in children aged 0-14. The aim of this analysis was to omit the use of a serological convenience sample and rely solely on representative data. The predicted probability of endemic transmission following importation was 1.44% (95%PI 1.01-1.99%), the median time to extinction of WPV1 following importation was 22.0 days (8-61).

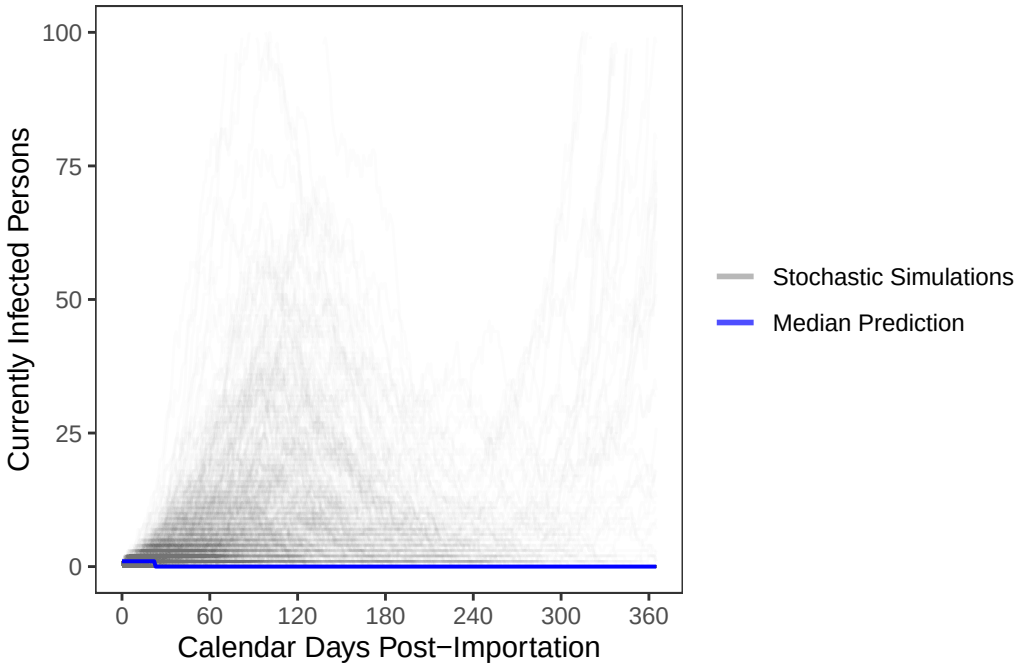

Figure S7: Stochastic dynamics of WPV1 transmission following importation. The predicted outbreak size and duration does not fundamentally differ from the main model, which included adults as well.

3 Model Fitting on the 2013 WPV1 Outbreak in Rahat, Israel

We adapted our model to fit it to WV1 wastewater CT measurements from the city of Rahat, Israel [13]. The purpose of this sensitivity analysis was to provide stronger justification for our parameter choices. For IPV-related parameters strongly based our parameter choices on an expert elicitation study. While existing polio have used these parameters, there is a lack of stronger empirical justification for their use. By fitting our model on a modern-day outbreak in a high-income country, we aimed to challenge our parameter choices.

3.1 Methods

3.1.1 Transmission Model

In the following system of ordinary differential equations, we again omit the ageing terms for simplicity During a vaccination campaign, targeted individuals move into waiting compartments. They transition out of these compartments at rate γ_w, at which point a fraction ϵ (dose efficacy) successfully seroconverts to the OPV class (V_o), while the remainder $(1-\epsilon)$ return to their previous immunity state. Let $c_g(t)$ represent the campaign vaccination rate for age group g at time t, the the susceptible, IPV vaccinated, and exposed compartments follow

$$\frac{dS_g}{dt} = b_g - \nu_g S_g - c_g(t)S_g - \lambda_{s,g}(\mathbf{I})S_g - \mu S_g + \gamma_w(1-\epsilon)W_{s,g} \tag{18}$$

$$\frac{dV_{i,g}}{dt} = \nu_g S_g - c_g(t)V_{i,g} - \lambda_{i,g}(\mathbf{I})V_{i,g} - \mu V_{i,g} + \gamma_w(1-\epsilon)W_{vi,g} \tag{19}$$

$$\frac{dW_{s,g}}{dt} = c_g(t)S_g - \lambda_{s,g}(\mathbf{I})W_{s,g} - (\gamma_w + \mu)W_{s,g} \tag{20}$$

$$\frac{dW_{vi,g}}{dt} = c_g(t)V_{i,g} - \lambda_{i,g}(\mathbf{I})W_{vi,g} - (\gamma_w + \mu)W_{vi,g} \tag{21}$$

$$\frac{dV_{o,g}}{dt} = \gamma_w\epsilon W_{s,g} + \gamma_w\epsilon W_{vi,g} - \lambda_{o,g}(\mathbf{I})V_{o,g} - \mu V_{o,g} \tag{22}$$

$$\frac{dE_{s,g}}{dt} = \lambda_{s,g}(\mathbf{I})(S_g + W_{s,g}) - \sigma E_{s,g} - \mu E_{s,g} \tag{23}$$

$$\frac{dE_{i,g}}{dt} = \lambda_{i,g}(\mathbf{I})(V_{i,g} + W_{vi,g}) - p_i\sigma E_{i,g} - \mu E_{i,g} \tag{24}$$

$$\frac{dE_{o,g}}{dt} = \lambda_{o,g}(\mathbf{I})V_{o,g} - p_o\sigma E_{o,g} - \mu E_{o,g} \tag{25}$$

The Erlang-distributed shedding stages remain largely unchanged, but the inflows for IPV and OPV vaccinated individuals are now scaled by p_i and p_o based on the outflows defined above.

For individuals originating from the susceptible pathway (S) the infection dynamics follow

$$\frac{dI^{(1)}_{a,s,g}}{dt} = p_s\sigma E_{s,g} - (\gamma_{a,s,1} + \mu)I^{(1)}_{a,s,g} \tag{26}$$

$$\frac{dI^{(k)}_{a,s,g}}{dt} = \gamma_{a,s,k-1}I^{(k-1)}_{a,s,g} - (\gamma_{a,s,k} + \mu)I^{(k)}_{a,s,g} \quad \text{for } k \in \{2,3\} \tag{27}$$

$$\frac{dI^{(1)}_{d,s,g}}{dt} = (1-p_s)\sigma E_{s,g} - (\gamma_{d,s,1} + \mu_d)I^{(1)}_{d,s,g} \tag{28}$$

$$\frac{dI^{(k)}_{d,s,g}}{dt} = \gamma_{d,s,k-1}I^{(k-1)}_{d,s,g} - (\gamma_{d,s,k} + \mu_d)I^{(k)}_{d,s,g} \quad \text{for } k \in \{2,3\} \tag{29}$$

For individuals from the vaccinated pathways (V_i and V_o):

$$\frac{dI^{(1)}_{a,i,g}}{dt} = p_i\sigma E_{i,g} - (\gamma_{a,i,1} + \mu)I^{(1)}_{a,i,g} \tag{30}$$

$$\frac{dI^{(k)}_{a,i,g}}{dt} = \gamma_{a,i,k-1}I^{(k-1)}_{a,i,g} - (\gamma_{a,i,k} + \mu)I^{(k)}_{a,i,g} \quad \text{for } k \in \{2,3\} \tag{31}$$

$$\frac{dI^{(1)}_{a,o,g}}{dt} = p_o\sigma E_{o,g} - (\gamma_{a,o,1} + \mu)I^{(1)}_{a,o,g} \tag{32}$$

$$\frac{dI^{(k)}_{a,o,g}}{dt} = \gamma_{a,o,k-1}I^{(k-1)}_{a,o,g} - (\gamma_{a,o,k} + \mu)I^{(k)}_{a,o,g} \quad \text{for } k \in \{2,3\} \tag{33}$$

The Recovered compartment gathers all inflows and is dervied as

$$\frac{dR_g}{dt} = \gamma_{a,s,3}I^{(3)}_{a,s,g} + \gamma_{d,s,3}I^{(3)}_{d,s,g} + \gamma_{a,i,3}I^{(3)}_{a,i,g} + \gamma_{a,o,3}I^{(3)}_{a,o,g} - \mu R_g. \tag{34}$$

In our model, we convert the shedding population fraction to a PCR C_t value. Let $w_{m,k}$ be the relative shedding weight for immunity status m in infection stage k, and $N(t)$ be the total living population at time t. The effective shedding weight $P_{shed}(t)$, is calculated as

$$P_{shed}(t) = \frac{1}{N(t)}\sum_g \sum_{k=1}^{3} \left(w_{s,k}\left(I^{(k)}_{a,s,g} + I^{(k)}_{d,s,g}\right) + w_{i,k}I^{(k)}_{a,i,g} + w_{o,k}I^{(k)}_{a,o,g}\right), \tag{35}$$

where each infected compartment is weighted by how much virus it sheds relative to others.

The simulated cycle threshold, $C_t(t)$, given a scaling parameter κ, is bounded between 0 and the limit of detection (60 PCR cycles) such that

$$C_t(t) = \min\left(\max\left(\log_2\left(\frac{\kappa}{P_{shed}(t)}\right), 0\right), 60\right). \tag{36}$$

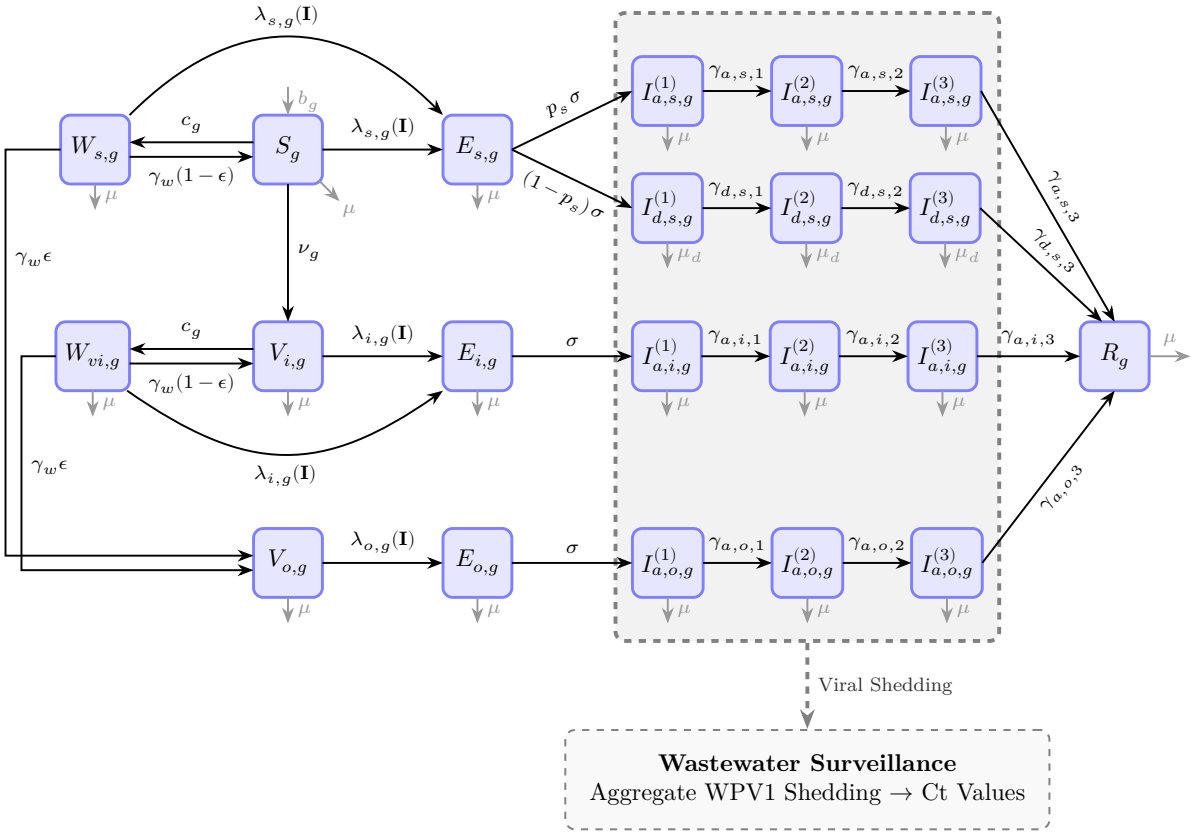

Figure S8: Schematic diagram of the Poliovirus transmission model that was used to fit the outbreak in Rahat, Israel. We added transitions for the OPV vaccination campaign and a link from viral shedding to wastewater surveillance to our baseline model. Upon receipt of a dose of OPV, people can transition into the waiting compartments. Their underlying immunity status does not change there. After the waiting time, people either have a successful immune response (transition into OPV stream), or they return to their previous compartments. The arrows from infectious compartments back to the force of infection were omitted to reduce visual clutter. The model was fitted on Rt-PCR cycle thresholds (C_t) values of WPV1 in wastewater.

3.1.2 Parameters

Since our primary interest are the IPV-related parameters, and whether our choices were justifiable, we kept the set of fitted parameters small. Fitting the full parameter set to this short time series of wastewater measurements would result in un-identifiability and collinearity issues (e.g. the same epidemic curve can be fitted by high IPV-shedding and high vaccine effectiveness (VE), or by low shedding and low VE). The variables with the largest assumed uncertainty were fitted.

Table S10: Fixed parameters of the model before fitting to the outbreak.

Parameter	**Best Estimate**	**References**
Latent period (days)	3	[15, 16]
Probability of AFP	1/200	[17]
Total mortality rate of AFP	10%	[17]
Total shedding duration (days)		[13, 18, 19]
Susceptibles	29	
IPV vaccinated	18	
Relative duration of infection stages		[13, 18]
Stage 1	$4/29$	
Stage 2	$3/29$	
Stage 3	$22/29$	
Relative shedding intensity in infection stages		[13, 18]
Stage 1	$10^{1.3}/10^{2.5}$	
Stage 2	1	
Stage 3	$10^{1.3}/10^{2.5}$	
OPV effectiveness against infection	80%	[18]
Shedding of WPV1 infection in OPV vaccinated persons relative to susceptibles	0.05	[14, 18]
Seasonal forcing amplitude	0.0	[11, 12]
OPV Vaccination Campaign		[11, 13]
Campaign 1 start (calendar day)	216	
Campaign 1 end (calendar day)	247	
Campaign 2 start (calendar day)	279	
Campaign 2 end (calendar day)	289	
Vaccination rate per capita per day	0.074	
Dose efficacy of OPV vaccination	0.63	

Table S11: Fitted parameters and their weakly informative prior distributions.

Parameter	**Prior Distribution**	**References**
R_0	$\mathcal{U}(1.1, 7.0)$	[14]
Number of infected persons on March 11	$\mathcal{U}(1, 500)$	[12]
Environmental scaling factor (κ)	$\mathcal{U}(10^5, 10^7)$	[13]
IPV vaccine effectiveness against infection	$\mathcal{U}(0, 0.5)$	[18]
Relative infectiousness of IPV-vaccinated individuals	$\mathcal{U}(0.01, 0.5)$	[14, 18]

3.1.3 Approximate Bayesian Computation

To estimate the joint posterior distribution of the unobserved parameters, we used Approximate Bayesian Computation with Sequential Monte Carlo sampling (ABC-SMC). The model was calibrated using weekly RT-PCR cycle threshold (C_t) values of WPV1 in wastewater samples from Rahat, Israel, during the 2013 outbreak.

Let $C_{t,\text{obs}}(t)$ represent the observed cycle threshold value at day t, and $C_{t,\text{sim}}(t;\theta)$ represent the simulated cycle threshold value generated by the model under parameter set θ. Because cycle threshold values are inversely proportional to log-transformed viral concentrations, we transformed both observed and simulated C_t values to a $\log_{10}$ concentration scale. The limit of detection was 60 cycles [13]. The transformed values represent relative log-concentrations:

$$\text{conc}_{\text{obs}}(t) = (60 - C_{t,\text{obs}}(t)) \log_{10}(2) \tag{37}$$

$$\text{conc}_{\text{sim}}(t;\theta) = (60 - C_{t,\text{sim}}(t;\theta)) \log_{10}(2) \tag{38}$$

A weighted sum of squared errors was used as our distance metric $d(\mathbf{y}_{\text{obs}}, \mathbf{y}_{\text{sim}}(\theta))$ across all observation days $t \in T$

$$d(\mathbf{y}_{\text{obs}}, \mathbf{y}_{\text{sim}}(\theta)) = \sum_{t \in T} w(t) \cdot e(t)^2, \tag{39}$$

where the error was adjusted to account for observations that fall below the limit of detection

$$e(t) = \begin{cases} 0 & \text{if } C_{t,\text{obs}}(t) \geq 60 \text{ and } C_{t,\text{sim}}(t;\theta) \geq 60 \\ |\text{conc}_{\text{sim}}(t;\theta) - \text{conc}_{\text{obs}}(t)| & \text{otherwise} \end{cases} \tag{40}$$

To prioritize fitting periods of high viral load, where the signal-to-noise ratio is best, the squared errors were weighted proportionally to the measured concentration in wastewater

$$w(t) = \text{conc}_{\text{obs}}(t) + 1. \tag{41}$$

The primary purpose of this sensitivity analysis was to provide a sensitivity analysis for our model assumptions for Germany, especially regarding IPV vaccination. Unidentifiability of these parameters from data is an issue, which is why we mapped IPV vaccine effectiveness and shedding by IPV vaccinated persons into a single joint risk score

$$J_i = (1 - \eta_i) \times r_i. \tag{42}$$

This joint parameter J_i represents the expected relative contribution of an IPV-vaccinated person to the overall viral load in wastewater. Because different combinations of high efficacy/high shedding and low efficacy/low shedding yield identical joint risk values (contour lines across the parameter space), we would not be able to distingiush between these parameter combinations with the available data.

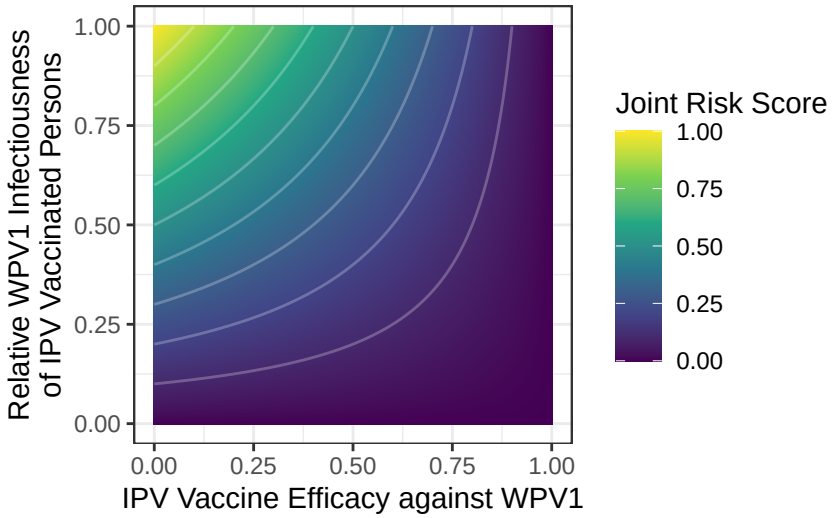

Figure S9: Joint risk score J_i of IPV vaccine effectiveness against WPV1 infection, and reduction in WPV1 shedding by IPV vaccinated persons. These two paramters would not be identifiable reliably using ABC-SMC, but the joint score collapses them into a single dimension, making posterior convergence easier.

3.2 Results

3.2.1 Posterior Distributions

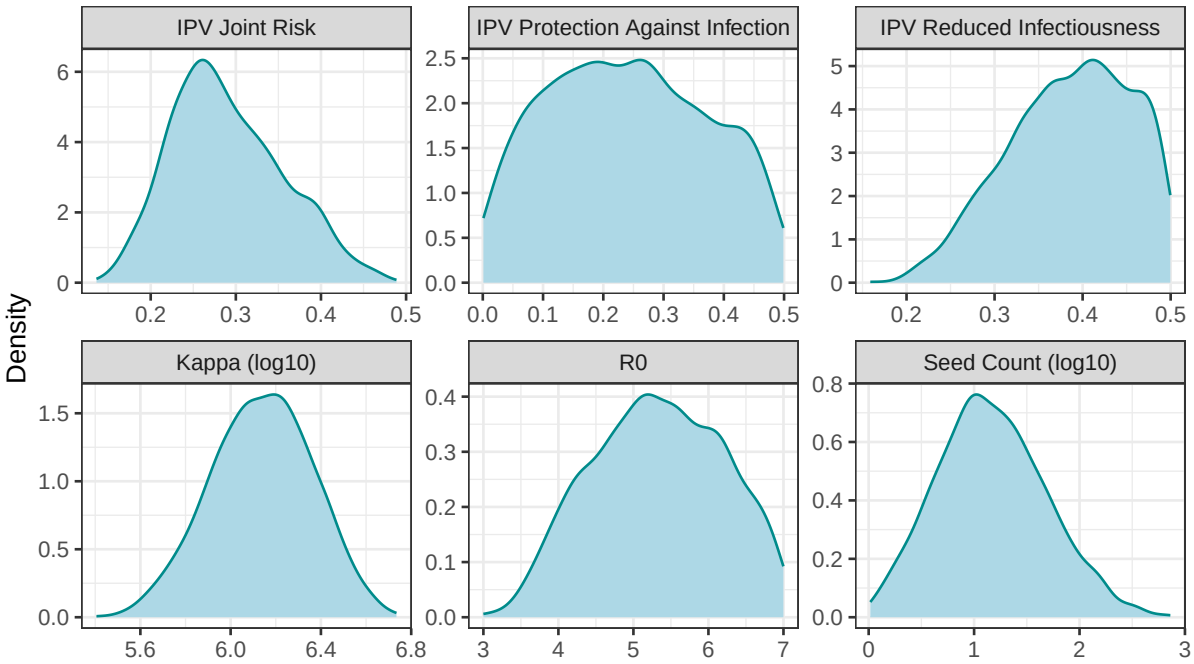

Figure S10: Posterior distribution of fitted parameters. Shaded areas represent kernel density estimates for vaccine-related parameters (top row: IPV protection against infection, IPV reduced infectiousness, and the combined IPV contribution to transmission (J_i)) and transmission dynamics parameters (bottom row: wastewater decay parameter $\log_{10}\kappa$, basic reproduction number R_0, and $\log_{10}$ of the initial seed count). The individual IPV-related parameters are not reliably identifiable from the data and the posteriors show high parameter uncertainty. The combined contribution to transmission parameter J_i forms a well-defined posterior distribution.

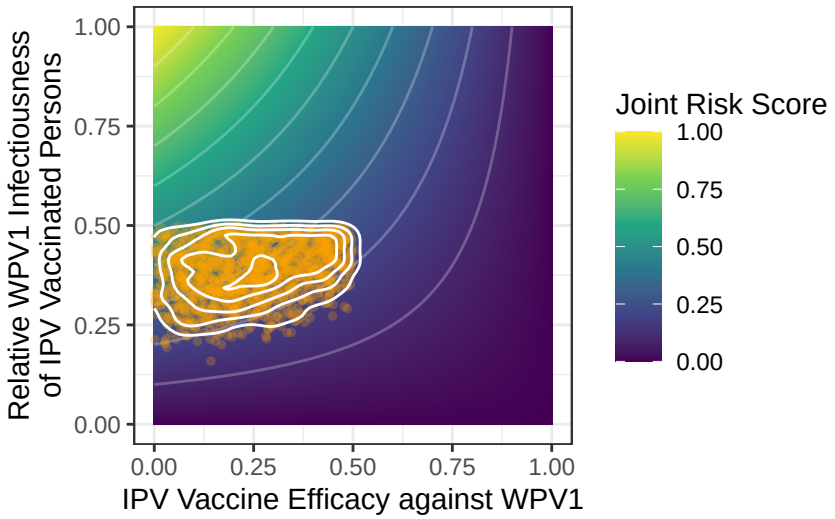

Figure S11: Joint risk score of IPV vaccine effectiveness against WPV1 infection, and reduction in WPV1 shedding by IPV vaccinated persons. The orange dots and white contours represent the accepted ABC particles and their position in the parameter plane.

3.2.2 Posterior Predictive Simulation

We used the fitted parameters for a posterior predictive simulation of the outbreak in Israel. The fitted model closely matched the observed wastewater data.

In a next step, we used the posterior distributions of IPV vaccine effectiveness and shedding with the reference scenario for imported WPV1 in Germany. This posterior predictive simulation for Germany resulted in a more pessimistic prediction, with a 13.3% (95%PI 11.7-15.1%) probability of an AFP case following importation. The probability of endemic transmission was estimated at 15.5% (95%PI 13.7-17.6%).

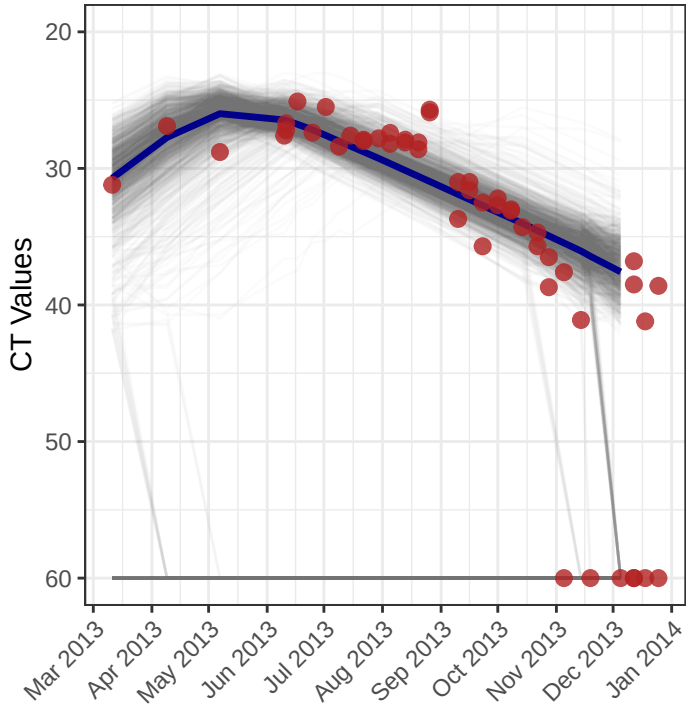

Figure S12: Posterior predictive simulation of the wastewater detections in Rahat, Israel. The red dots are the wastewater WPV1 RT-PCR Cycle Threshold (CT) values. The grey lines are 2500 posterior predictive simulations, and the blue line is their median.

3.3 Discussion

The fitting of the model to the wastewater PCRs from Rahat, Israel was done to validate the model structure and provide a sensitivity analysis to the chosen IPV-related parameters (vaccine effectiveness (VE) and reduction in WPV1 shedding).

This sensitivity analysis however has several limitations:

- **Parameter Unidentifiability and Collinearity:** Individual IPV-related parameters, vaccine efficacy against infection (η_i) and relative infectiousness/shedding (r_i), cannot be disentangled from wastewater cycle threshold (C_t) data alone. High efficacy paired with high shedding yields the same wastewater dynamics as low efficacy paired with low shedding. Consequently, only the composite joint risk score $J_i = (1 - \eta_i) \times r_i$ could be reliably constrained when fitting the model on the wastewater time series.
- **Loss of Granularity from Wastewater Data:** Wastewater surveillance yields an aggregated, community-wide viral shedding signal. Crucially, this lacks information on vaccination status of the shedding persons. Knowing the IPV vaccinated fraction of the population [31] allows to fit a rough estimate of vaccination-related parameters using our model, but reliable and precise estimation of those parameters is not possible.
- **Dependence on Fixed Parameter Assumptions:** To achieve convergence and avoid collinearity across the entire parameter space, several parameters (e.g., total shedding duration, OPV campaign timing and dose efficacy) were held fixed. Mis-specification in these parameters could shift the estimated posteriors of the fitted parameters.
- **Setting and Structural Mismatches:** Rahat represents a unique demographic and social context (i.e. a densely connected Bedouin community). Direct translation of transmission dynamics to Germany introduces potential ecological bias, given potential differences in mixing patterns, importance of fecal and oro-pharyngeal transmission pathways, and sanitation infrastructure.

Despite these limitations, this sensitivity analysis is important for our evaluation of WPV1 transmission risks in Germany:

- **Validates Model Structure:** The fit to the Rahat wastewater trajectory demonstrates that the underlying modelling framework is capable of capturing real-world WPV1 outbreak dynamics.
- **Sensitivity to IPV Protection:** The predictions following WPV1 importations are sensitive to the assumed vaccine efficiacy and reduction in shedding from IPV vaccinated persons. For better predictions in the German context, more data is needed on the effect that IPV has on WPV1 transmission dynamics.
- **Pessimistic Risk Bound:** When parameter sets drawn from the Israel posterior distribution were applied to the German reference importation scenario, the predicted probability of endemic transmission rose sharply to about 15%. This is significantly more pessimistic than the predictions using paramters from the expert elicitation study.

However, due to the limitations of the sensitivity analysis discussed above, this should be interpreted as a conservative upper risk bound for the German context.

- **Emperical Grounding of Scenario Model:** Existing polio re-emergence scenario models did not attempt fitting their models on real-world outbreaks as part of sensitivity analyses [9, 10, 20, 26, 29]. By fitting our model on a wastewater time-series we aim to improve the empirical grounding of our scenario model for Germany.

References

[1] Niko Kohmer, Holger F Rabenau, Veronika Rilling, Sandra Ciesek, Martin Enders, and Maren D. Eggers. Polio type 2 and 3 eradication: Relevance to the immunity status of individuals living in germany, 2005-2020. *Journal of clinical virology : the official publication of the Pan American Society for Clinical Virology*, 164:105471, 2023.

[2] Grace R. Macklin, Grace R. Macklin, Nicholas C. Grassly, Roland W. Sutter, Ondrej Mach, Ananda Sankar Bandyopadhyay, W. John Edmunds, and Kathleen M. O'Reilly. Vaccine schedules and the effect on humoral and intestinal immunity against poliovirus: a systematic review and network meta-analysis. *The Lancet. Infectious diseases*, 2019.

[3] Nicholas C. Grassly. Immunogenicity and effectiveness of routine immunization with 1 or 2 doses of inactivated poliovirus vaccine: Systematic review and meta-analysis. *The Journal of Infectious Diseases*, 210:S439 – S446, 2014.

[4] Sabine Diedrich, Hermann Claus, and Eckart Schreier. Immunity status against poliomyelitis in germany: Determination of cut-off values in international units. *BMC Infectious Diseases*, 2:2 – 2, 2002.

[5] R. Kettlitz, M. Harries, S. Contreras, J. Reinecke, M. S. Wieder, T. von Lengerke, S. Castell, B. Lange, C. J. Klett-Tammen, V. Melhorn, D. A. Schulze, F. J. Helmholtz, and I. Rodiah. Self-reported poliomyelitis vaccination and documentation in adults indicates high uptake: a digital German epidemic panel, December 2024. *BMC Public Health*, 25(1):3514, 2025.

[6] Stan Development Team. *Stan User's Guide*, 2026. Accessed: 2026-08-03.

[7] Daniel P. Simpson, Haavard Rue, Thiago G. Martins, Andrea Riebler, and Sigrunn Holbek Sørbye. Penalising model component complexity: A principled, practical approach to constructing priors. *Statistical Science*, 32:1–28, 2014.

[8] Stefan Lang and Andreas Brezger. Bayesian p-splines. *Journal of Computational and Graphical Statistics*, 13:183 – 212, 2004.

[9] Tara D Mangal, Raymond Bruce Aylward, and Nicholas C. Grassly. The potential impact of routine immunization with inactivated poliovirus vaccine on wild-type or vaccine-derived poliovirus outbreaks in a posteradication setting. *American journal of epidemiology*, 178 10:1579–87, 2013.

[10] Megan Auzenbergs, Kaja Abbas, Corey M Peak, Arend Voorman, Mark Jit, and Kathleen M. O'Reilly. Vaccination strategies against wild poliomyelitis in polio-free settings: outbreak risk modelling study and cost-effectiveness analysis. *BMJ Global Health*, 10, 2025.

[11] Rami Yaari, Ehud Kaliner, Itamar Grotto, Guy Katriel, Jacob Moran-Gilad, Danit Sofer, Ella Mendelson, Elizabeth Miller, and Amit Huppert. Modeling the spread of polio in

an ipv-vaccinated population: lessons learned from the 2013 silent outbreak in southern israel. *BMC Medicine*, 14, 2016.

[12] Andrew F. Brouwer, Joseph N. S. Eisenberg, Connor D. Pomeroy, Lester M. Shulman, Musa Hindiyeh, Yossi Manor, Itamar Grotto, James S. Koopman, and Marisa C. Eisenberg. Epidemiology of the silent polio outbreak in rahat, israel, based on modeling of environmental surveillance data. *Proceedings of the National Academy of Sciences*, 115:E10625 – E10633, 2018.

[13] Andrew F. Brouwer, Marisa C. Eisenberg, Lester M. Shulman, Michael Famulare, James S. Koopman, Steve J Kroiss, Musa Hindiyeh, Yossi Manor, Itamar Grotto, and Joseph N. S. Eisenberg. The role of time-varying viral shedding in modelling environmental surveillance for public health: revisiting the 2013 poliovirus outbreak in israel. *Journal of the Royal Society Interface*, 19, 2022.

[14] Paul E M Fine and Ilona A Carneiro. Transmissibility and persistence of oral polio vaccine viruses: implications for the global poliomyelitis eradication initiative. *American journal of epidemiology*, 150 10:1001–21, 1999.

[15] Federal Centre for Health Education (BZgA). Pathogen fact sheet: Poliomyelitis (polio), 2023. Available in English; accessed July 2026.

[16] Centers for Disease Control and Prevention (CDC). Clinical overview of poliomyelitis. CDC Website, 2024. Accessed July 2026.

[17] World Health Organization. Poliomyelitis (polio) fact sheet. https://www.who.int/news-room/fact-sheets/detail/poliomyelitis, 2025. Accessed: July 13, 2026.

[18] Radboud J. Duintjer Tebbens, Mark A. Pallansch, Konstantin Chumakov, Neal A. Halsey, Tapani Hovi, Philip D. Minor, John F. Modlin, Peter A. Patriarca, Roland W. Sutter, Peter F. Wright, Steven G. F. Wassilak, Stephen L. Cochi, Jong-Hoon Kim, and Kimberly M. Thompson. Review and assessment of poliovirus immunity and transmission: Synthesis of knowledge gaps and identification of research needs. *Risk Analysis*, 33, 2013.

[19] James P. Alexander, Howard E. Gary, and Mark A. Pallansch. Duration of poliovirus excretion and its implications for acute flaccid paralysis surveillance: a review of the literature. *The Journal of infectious diseases*, 175 Suppl 1:S176–82, 1997.

[20] Kimberly M. Thompson, Dominika A. Kalkowska, and Radboud J. Duintjer Tebbens. Managing population immunity to reduce or eliminate the risks of circulation following the importation of polioviruses. *Vaccine*, 33:1568 – 1577, 2015.

[21] Thomas R Hird and Nicholas C. Grassly. Systematic review of mucosal immunity induced by oral and inactivated poliovirus vaccines against virus shedding following oral poliovirus challenge. *PLoS Pathogens*, 8, 2012.

[22] Radboud J. Duintjer Tebbens, Mark A. Pallansch, Dominika A. Kalkowska, Steven G. F. Wassilak, Stephen L. Cochi, and Kimberly M. Thompson. Characterizing poliovirus transmission and evolution: Insights from modeling experiences with wild and vaccine-related polioviruses. *Risk Analysis*, 33, 2013.

[23] Micaela Elvira Martinez-Bakker, Aaron A. King, and Pejman Rohani. Unraveling the transmission ecology of polio. *PLoS Biology*, 13, 2015.

[24] Kathrin Keeren, Sindy Böttcher, and Sabine Diedrich. Enterovirus surveillance (evsurv) in germany. *Microorganisms*, 9, 2021.

[25] Robert Koch-Institut. Inanspruchnahme von routineimpfungen in deutschland – ergebnisse aus der kv-impfsurveillance, 2026.

[26] James S. Koopman, Christopher J. Henry, Joonha Park, Marisa C. Eisenberg, Edward L. Ionides, and Joseph N. S. Eisenberg. Dynamics affecting the risk of silent circulation when oral polio vaccination is stopped. *Epidemics*, 20:21 – 36, 2017.

[27] Robert Koch-Institut. Rki-ratgeber: Poliomyelitis, 2026. Accessed: 2026-07-14.

[28] Olen Kew and Mark A. Pallansch. Breaking the last chains of poliovirus transmission: Progress and challenges in global polio eradication. *Annual review of virology*, 5 1:427–451, 2018.

[29] Radboud J. Duintjer Tebbens and Kimberly M. Thompson. Modeling the potential role of inactivated poliovirus vaccine to manage the risks of oral poliovirus vaccine cessation. *The Journal of infectious diseases*, 210 Suppl 1:S485–97, 2014.

[30] Richard Seager, David S. Battisti, J. Yin, Neil D. Gordon, Naomi Naik, Amy C. Clement, and Mark A. Cane. Is the gulf stream responsible for europe's mild winters? *Quarterly Journal of the Royal Meteorological Society*, 128, 2002.

[31] Binyamin Binyaminy, Natalya Bilenko, Eric J Haas, Itamar Grotto, and Michael Gdalevich. Socioeconomic status and vaccine coverage during wild-type poliovirus emergence in israel. *Epidemiology and Infection*, 144:2840 – 2847, 2016.